Understanding the activity of Zn-Cu sites in methanol synthesis

Batyrev, E.D.

Publication date
2013

Chapter 1

1 Introduction

1.1 Methanol

Methanol (CH_3OH, methyl alcohol) is a colorless, odorless, somewhat corrosive, and flammable liquid [1]. It was prepared in 1823 by condensing gases from burning wood. Methanol has been used for more than 100 years as a solvent and as a chemical building block for making plastics, plywood, and paints. Nowadays it is also used as an energy source, renewable when made from biomass, especially for fuel cell applications because of its high hydrogen content. Catalytic reforming of methanol is an efficient and environmentally attractive way to produce hydrogen.

1.2 Methanol economy

The industrial development was fuelled by coal, and later continued with oil, natural gas and nuclear energy. Today world's energy consumption is about 1.05×10^{18} calories per year (120 Petawatt-hours), equivalent to a continuous power consumption of about 13 terawatts (TW) [2].

With the rapidly increasing world population (Fig.1), higher standards of living, this demand for energy is expected to grow to 21 TW in 2025 and to about 30 TW in 2050 (Fig. 2).

When the fossil fuels (hydrocarbons) are used they form carbon dioxide and water and thus are not renewable on the human timescale. The proven oil reserve in 2003 was estimated 156.7 billion tones and natural gas reserve was 158.2 billion tones oil equivalent. Considering the growing population and accustomed level of comfort with the increased demand for hydrocarbons (> 80 million barrels/day oil and about 50 million barrels/day oil equivalent of gas) the reserves will last more than half a century. Not only the world population growth but also the increasing energy demands of China, India and other developing countries is already putting great pressure on the world's oil reserves. In view of the environmental dangers and concerns of safety of radioactive by-products the further development of atomic energy stands almost still. The Chernobyl accident [4] in 1986 and the Fukushima accident [4] in 2011 result in closing down of existing nuclear energy programs all over the world and some

countries are revising their energy programs. Last year, for example, Germany announced to shut all nuclear energy plants by 2022 [4].

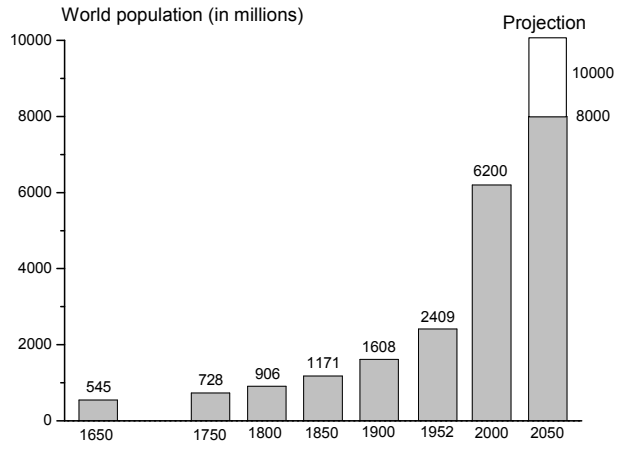

Fig. 1. *World population, 1650 projected to 2050, medium estimate (re-drawn after G.A. Olah et al. [2]). Source: United Nations, Population Division.*

It is obvious that the transition from the commonly used energy sources towards new energy technologies continues slowly; however, more opportunities are evolving and modern governmental policy nowadays favours the renewable fuel economy.

Synthetic oil is feasible [2], however the Fisher-Tropsch synthesis route is highly energy consuming, giving complex, unsatisfactory product mixtures, and therefore hardly be seen as the technology of the future.

The development of the biofuels [2], primarily by the fermentative conversion of the agricultural feedstock (derived from sugar cane and corn) to ethanol is evolving. Whereas the ethanol can be used as a gasoline additive or even alternative fuel, the enormous amounts of the transportation fuel needed clearly limit the applicability to specific countries and situations.

Methanol is considered as an alternative fuel that can decrease the current usage of the fossil fuels resulting in low CO_2 emission. Eventually, the emitted CO_2 by the power plants or even an atmospheric CO_2 can be recycled using catalytic process to produce methanol. The methanol is an efficient energy carrier for both internal combustion engine and fuel cell, as CH_3OH molecule is rich in

hydrogen. In liquid form it stores energy more conveniently and safely compared to hydrogen gas.

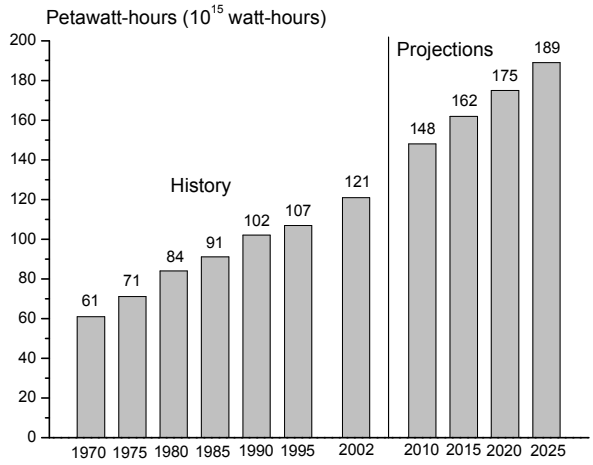

Fig. 2. *World primary energy consumption, 1970 to 2025 (re-drawn after G.A. Olah et al. [2]). Based on data from: Energy Information Administration (EIA), International Energy Outlook 2005.*

1.3 Commercial catalysts for methanol synthesis

Annual methanol production world-wide is a staggering 75 million metric tons [1]. It is industrially produced from synthesis gas ($CO/CO_2/H_2$), over a catalyst surface (1-2) under pressure of 50-100 bar and temperatures 473 – 523 K [5].

$$CO + 2H_2 = CH_3OH \qquad \Delta H_{298\,K} = -90.64 \text{ kJ/mol} \quad (1)$$

$$CO_2 + 3H_2 = CH_3OH + H_2O \qquad \Delta H_{298\,K} = -49.47 \text{ kJ/mol} \quad (2)$$

$$CO + H_2O = CO_2 + H_2 \qquad \Delta H_{298\,K} = -41.17 \text{ kJ/mol} \quad (3)$$

The catalysts contain a complex mixture of components. After activation these provide the surface features and mechanical properties necessary for a long, stable life. Today, the most active and selective commercial catalysts for the methanol synthesis consist of

about 55-60 wt% Cu with 25-30 wt% ZnO and 10 wt% Al_2O_3 as chemical and structural promoters [6, 7]. The unique formulation of the Johnson Matthey KATALCO 51-series catalyst is based on a copper-containing mineral in which a controlled proportion of the cations have been replaced by zinc ions [6]. The active phase is supported on a specifically designed zinc aluminate compound. The support provides a catalyst with good mechanical strength throughout operating life, while allowing reactant gases access to the active copper metal surface. Micro-crystalline zinc oxide is also present to protect the copper metal surface sites from poisons such as sulphur and chlorine compounds. Magnesia is added to modify the catalyst structure during manufacture to maximize activity throughout catalyst life.

Kinetic studies using isotope labelled carbon oxides [7-9] have demonstrated that under operating conditions methanol is produced by hydrogenation of CO_2 (2), where CO merely provides a source of CO_2 and acts as a reducing agent.

The value of the equilibrium constant for methanol formation (1-2) increases as temperature decreases and as pressure increases. This means that the highest conversion to methanol is achieved at high pressure and low temperature. The use of very high pressure in large scale is expensive both in terms of capital and compression costs. The novelty of the ICI Low Pressure Methanol (LPM) process (Fig. 3) when it was introduced was in the use of very active copper catalysts that allowed plants to operate at economic pressures and temperatures [6].

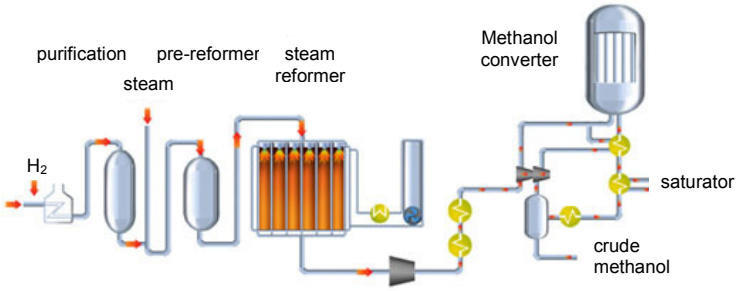

Fig. 3. *Operational scheme of the methanol process (re-drawn from Johnson Matthey Catalysts corporate brochure [6]).*

Fundamental work carried out by ICI on the synthesis of methanol from $CO_2/CO/H_2$ mixtures has shown that when using properly reduced supported copper catalysts:

– methanol is formed directly from the carbon dioxide, the concentration of which is affected by a complex set of competing reactions and *equilibria*.
– reaction takes place on active sites on the copper crystallites.
– the rate of reaction is a function of the copper surface area and, moreover, is dependent on the crystallography of the copper crystallites.
During reaction, active copper metal is partially oxidized by adsorbed oxygen. This condition has been shown to promote the adsorption of CO_2 and therefore affects reaction rate. The oxidation state of the copper metal surface depends on the ratio of CO to CO_2 in the synthesis gas. It is also known that at higher CO_2 to CO ratios, excessive surface oxidation can occur which appears to reduce the catalyst activity. This "loss" of activity is only temporary, as the oxidation of the surface is reversible on all KATALCO 51-series catalysts. It is most commonly seen when plants add extra CO_2 to the synthesis gas; with CO_2 addition, the activity appears to be slightly reduced; without CO_2 addition, the activity returns to normal.

KATALCO 51-1 and the LPM process revolutionised synthetic methanol production in the 1960s and have provided the majority of the world's production ever since that time. These technologies currently account for an annual production capacity of over 30 million tonnes of methanol. KATALCO 51-1 was the first three-component methanol synthesis catalyst comprising zinc oxide and alumina as the support with copper as the active catalytic component.

The high activity and stability of KATALCO 51-series catalysts means that typically a charge lasts between four and six years, but some charges have been in operation for more than 8 years. Their strength enables them to withstand the rigors of this extended operation and as a result they show little change in pressure drop and are easily discharged at the end of life.

1.4 Nature of the active site

An activation step is still required even for very active and selective catalysts. The Cu/ZnO catalytic system was massively studied in the last decades, but the nature of the active sites and the methanol synthesis mechanism are still under debate. We still don't know if the activity is determined only by available Cu surface [5-14] or also by the local structural environment of Cu (structure sensitivity). Klier *et al.* [15, 16] described that Cu^+ in solid solution with ZnO is the active species for methanol synthesis, whereas Okamoto *et al.* [17] concluded that Cu^0-Cu^+ species forming a two-

dimensional epitaxial layer on ZnO are catalytically active for methanol synthesis.

More recent studies have advocated for ZnO_x species on Cu with either Cu-Zn or Cu-O-Zn forming the active site [18, 19]. Choi and co-workers [20, 21] proposed that the Cu-Zn site is active for CO_2 hydrogenation and Cu-O-Zn is active for CO hydrogenation. Extremely surface sensitive Low Energy Ion Scattering (LEIS) work revealed an enrichment of the surface in ternary $Cu/ZnO/SiO_2$ catalyst by ZnO_x species [22].

According to French *et al.* the ZnO is an anti-sintering agent, and even an active site [23], but does not influence metallic Cu as the site for CO_2 hydrogenation [24].

A positive correlation was found between a strain in Cu nanoparticles induced by the ZnO support with methanol synthesis turnover frequency [25]. The observation of strain in Cu nanoparticles has more recently been confirmed by an *in situ* Electron Energy Loss Spectroscopy (EELS) study [26]. The debate is still ongoing with more reports of structure sensitivity of methanol synthesis emerging from other *in situ* techniques. Grunwaldt *et al.* [27] demonstrated a correlation between catalyst activity, synthesis gas reduction potential, and apparent Cu coordination number as determined by *in situ* Extended X-ray Absorption Fine Structure (EXAFS) spectroscopy. They interpreted the (reversible) change in coordination number as a shape change of the nanometer sized Cu crystallites, exposing facets of different catalytic activity. This Cu transformation dependence on synthesis gas reduction potential has been confirmed later by *in situ* High Resolution Transmission Electron Microscopy (HR-TEM) study [28].

There is a wide agreement that the oxide catalyst formed by calcining co-precipitated (Cu, Zn) hydroxycarbonates contains ZnO with Cu in solid solution. Copper migrates to the ZnO surface during the reduction process, forming dispersed structures with particularly high catalytic activity [29-34]. Stirling *et al.* [31] found that a maximum of about 1 mol % CuO can dissolve in ZnO, for catalysts calcined at 1053 K – 1173 K. Whereas Ketchik *et al.* [29] showed that ZnO in catalysts calcined at 623 K may contain up to 10 mol % CuO in solid solution. Klenov *et al.* [35] and Yurieva *et al.* [36] suggested that, using a combination of HR-TEM and X-Ray Diffraction (XRD) measurements and simulations, the Cu-doped ZnO contains a large number of stalking-fault defects along the (001) plane and that Cu atoms are primarily located close to these defects.

Based on the literature overview above, three main theories may be distinguished concerning the active state of copper in Cu/ZnO-based catalysts, *viz.* Cu^0, Cu^+, and a Cu/Zn alloy [11, 16, 21]. They are

wetting/non-wetting model of ZnO by metallic Cu [27, 28], flat epitaxial Cu particles on top of ZnO balanced by dissolved protons [32], and Cu particles or mixed oxide covered by ZnO_x species [22].

Importantly, the surface structure of the catalyst should be activated in hydrogen at high temperature prior to the methanol synthesis. Brands *et al.* [37] found that supported $Cu/ZnO/SiO_2$ catalysts reduced at high temperature exhibited a profound increase in the rate of methanol synthesis, as well as ester hydrogenolysis. The conclusion from this [37] and other works [38–40] is that the Cu–ZnO interface is crucial for the activation of carbonyl functions towards hydrogenation, possibly involving stabilisation of Cu^+ [16]. In a recent LEIS study, Jansen *et al.* reported that the surface composition of a similar $^{63}Cu/^{68}ZnO/SiO_2$ catalyst depends strongly on the applied reduction temperature [22].

My study is focused on the surface sites of activated catalyst that will later on be exposed to syngas mixture for the methanol synthesis. In course of this work a combination of surface science techniques with classical characterisation methods is applied.

1.5 Surface and structural approach to the active sites

The surface and structural studies above are dealing with the Cu/ZnO catalysts prepared by different methods and sometimes with the structural promoters such as Al_2O_3. This difference in catalyst preparation/structure in combination with the different reaction/reduction conditions may lead to the formation of various surface sites and therefore various reaction routes could be proposed. This increases the number of puzzles in the already complex nature of the active sites in methanol synthesis.

The structural analysis of Cu/ZnO modification in highly active silica [41] supported Cu/ZnO catalyst was used as a learning platform. In course of our structural investigation of $Cu/ZnO/SiO_2$ catalyst structure, the Cu/ZnO content ratio and the gas pressure was kept the same, while only the temperature was a varying parameter.
Based on the obtained knowledge we switched from the powder catalyst to model system to visualize the Cu-Zn interaction in nanoscopic scale [42, 43]. Therefore the Cu nanoclusters deposited on ZnO-(0001) surface were probed by surface sensitive techniques such as Scanning Tunneling Microscopy (STM), Scanning Tunneling Spectroscopy (STS), X-ray Photoelectron Spectroscopy (XPS) and Temperature Programmed Desorption (TPD). Again the temperature was only changing factor in this study.

1.5.1 Classical characterization techniques

1.5.1.1 Thermogravimetry and N_2O chemisorption

Thermogravimetry (TGA) measures the amount of weight change of a material, either as a function of increasing temperature, or isothermally as a function of time, in an atmosphere of nitrogen, helium, air, other gas, or in vacuum.

Sample weight ranges from 1 mg to 150 mg routinely. Sample weights of more than 25 mg are preferred, but excellent results are sometimes obtainable on 1 mg of material. Weight change sensitivity of the TGA setup is 0.01 mg. Samples can be analyzed in the form of powder or small pieces so the interior sample temperature remains close to the measured gas temperature.

This method allows quantitative composition analysis and analysis of reactions with air, oxygen, or other reactive gases. The reacted material can then be identified by XPS and/or microscopy.

The activated metal surface is usually treated with N_2O at 363 K to determine the metal surface area available for the reaction. The N_2O mildly passivates the outermost metallic layer and the oxygen uptake is directly proportional to the metal sites that were involved in the oxidation.

1.5.1.2 *In situ* X-ray Diffraction (XRD)

X-ray crystallography is a method for determining the atomic and molecular structure of a crystal, in which the crystalline atoms cause a beam of X-rays to diffract into many specific directions (Fig. 4). By measuring the angles and intensities of these diffracted beams, a crystallographer can produce a three-dimensional picture of the density of electrons within the crystal. From this electron density, the mean positions of the atoms in the crystal can be determined, as well as their chemical bonds, their disorder and various other information.

Crystals are regular arrays of atoms, and X-rays can be considered as waves of electromagnetic radiation. Atoms scatter X-ray waves, primarily through the atom's electrons. Just as an ocean wave striking a lighthouse produces secondary circular waves emanating from the lighthouse, so an X-ray striking an electron produces secondary spherical waves emanating from the electron. This phenomenon is known as elastic scattering, and the electron (or lighthouse) is known as the scatterer. A regular array of scatterers produces a regular array of spherical waves. Although these waves cancel one another out in most directions through destructive

interference, they add constructively in a few specific directions, determined by Bragg's law:

$$2d \sin\theta = n\lambda \qquad (4)$$

Here d is the spacing between diffracting planes, θ is the incident angle, n is any integer, and λ is the wavelength of the beam. These specific directions appear as spots on the diffraction pattern called reflections. Thus, X-ray diffraction results from an electromagnetic wave (the X-ray) impinging on a regular array of scatterers (the repeating arrangement of atoms within the crystal).

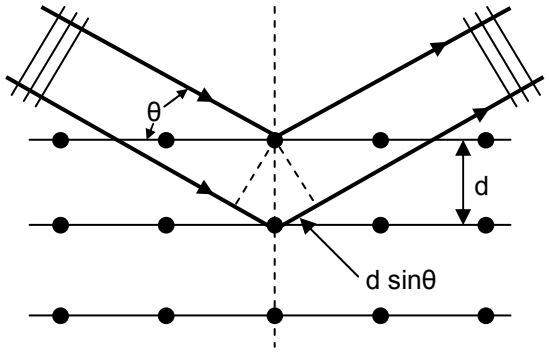

Fig. 4. *Bragg diffraction from a cubic crystal lattice. Plane waves incident on a crystal lattice at angle θ are partially reflected by successive parallel crystal planes of spacing d. The superposed reflected waves interfere constructively if the Bragg condition (4) is satisfied.*

X-ray crystallography is related to several other methods for determining atomic structures. Similar diffraction patterns can be produced by scattering electrons or neutrons, which are likewise interpreted as a Fourier transform. If single crystals of sufficient size cannot be obtained, various other X-ray methods can be applied to obtain less detailed information; such methods include fiber diffraction, powder diffraction and small-angle X-ray scattering (SAXS). If the material under investigation is only available in the form of nanocrystalline powders or suffers from poor crystallinity, the methods of electron crystallography can be applied for determining the atomic structure.

For all the above mentioned X-ray diffraction methods, the scattering is elastic; the scattered X-rays have the same wavelength as the incoming X-ray. By contrast, *inelastic* X-ray scattering methods are useful in studying excitations of the sample, rather than the distribution of its atoms.

1.5.1.3 Extended X-ray Absorption Fine Structure (EXAFS)

With the availability of the synchrotron radiation sources, X-ray absorption spectroscopy techniques (XAS) developed into widely used tools for the structural research of materials by identifying the local structure around atoms of a selected type in the sample. In EXAFS number and species of neighbour atoms, their distance from the selected atom and the thermal or structural disorder of their positions can be determined from the oscillatory part of the absorption coefficient above a major absorption edge. The analysis can be applied to crystalline, nanostructural or amorphous materials, liquids and molecular gases. EXAFS is often the only practical way to study the arrangement of atoms in materials without long range order, where traditional diffraction techniques cannot be used. High resolution X-ray absorption spectroscopy (XAS), that became available with the development of synchrotron radiation sources, has introduced powerful experimental methods for the investigation of atomic and molecular structures of materials. With the synchrotron radiation high-flux monochromatic X-ray beams with the energy resolution $\Delta E/E$ of the order of 10^{-4} are easily obtainable, allowing measurements of high quality absorption spectra in a short time. In a typical experimental set-up (Fig. 5) ionisation cells monitor the intensity of incident (I_0) and transmitted (I_1) monochromatic photon beam through the sample.

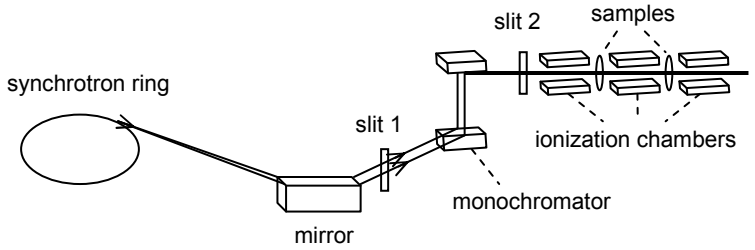

Fig. 5. *Schematic view of E4 X-ray beamline at Hamburger Synchrotron Radiation Laboratory (HASYLAB) at DESY in Hamburg.*

With the well-known exponential attenuation of X-rays in a homogeneous medium, the absorption coefficient $\mu(E)$ at a given photon energy E can be obtained from the relation $\mu = \ln(I_1/I_0)/d$, where d is the sample thickness. The energy dependence of the absorption coefficient is collected by a stepwise scan of the photon energy in the monochromatic beam with the Bragg monochromator.

1.5.1.4 Small Angle Neutron Scattering (SANS)

SANS is an experimental technique that uses elastic neutron scattering at small scattering angles to investigate the structure of various substances at a mesoscopic scale of about 1 - 1000 nm.

During a SANS experiment a beam of neutrons is directed at a sample, which can be an aqueous solution, a solid, a powder, or a crystal. The neutrons are elastically scattered by nuclear interaction with the nuclei or interaction with magnetic momentum of unpaired electrons. In X-ray scattering, photons interact with electrical cloud so the bigger the element, the bigger the effect. But in neutron scattering, neutron interacts with nuclei and interaction depends on isotope and some light elements like deuterium show similar scattering cross section as heavy elements like Pb.

In zero order dynamical theory of diffraction, the refractive index is directly related to the scattering length density and is a measure of the strength of the interaction of a neutron wave with a given nucleus. The following table shows the scattering lengths for various elements (in 10^{-12} cm) [44].

H	D	C	N	O	P	S
-0.3742	0.6671	0.6651	0.940	0.5804	0.517	0.2847

Note that the relative scale of the scattering lengths is the same. Another important point is that the scattering from hydrogen is distinct from that of deuterium. Hydrogen is one of the few elements that has a negative scatter, which means that neutrons deflected from hydrogen are 180° out of phase relative to those deflected by the other elements. These features are important for the technique of contrast variation. Small angle neutron scattering is in many respects very similar to small-angle X-ray scattering (SAXS); both techniques are jointly referred to as small-angle scattering (SAS). Advantages of SANS over SAXS are its sensitivity to light elements, the possibility of isotope labelling, and the strong scattering by magnetic moments.

1.5.2 Surface sensitive techniques

Development of new surface sensitive techniques in the second half of the 20th century has resulted in huge technological boost in many surface related applications such as coatings, electronics, catalysis, etc.

In 1969 a first commercial XPS instrument was built up at Hewlett Packard based on the method significantly improved by K.

Sigbahn [45]. In 1971 R. Young and his co-workers have published paper [46], where they describe how to acquire the surface topography with the usage of current between surface and sharp metallic tip. Later in 1982, G. Binnig and H. Rohrer have patented the development of scanning tunnelling microscope [47] and this powerful technique led to an enormous growth of the surface studies in last decades.

1.5.2.1 Scanning Tunneling Microscopy (STM)

Scanning tunnelling microscopy is a technique developed in the eighties and provides images of solid surfaces with unprecedented resolution. The operation of a scanning tunnelling microscope (STM) is based on the so-called tunnelling current, which starts to flow when a sharp tip approaches a conducting surface at a distance of approximately one nanometre. The tip is mounted on a piezoelectric tube, which allows tiny movements by applying a voltage at its electrodes (Fig. 6). Thereby, the electronics of the STM system

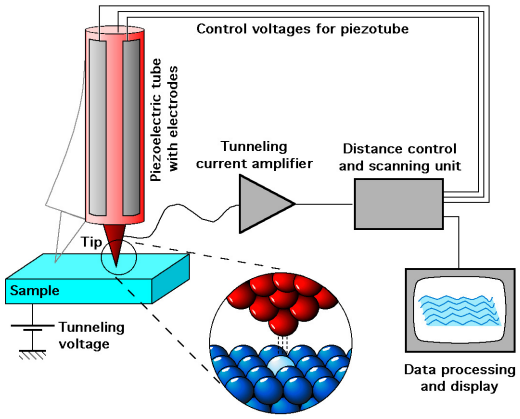

Fig. 6. *Schematic diagram of a scanning tunnelling microscope (adapted from Dr. M. Schmid, TU Wien [48]).*

control the tip position in such a way that the tunnelling current and, hence, the tip-surface distance is kept constant, while at the same time scanning a small area of the sample surface. This movement is recorded and can be displayed as an image of the surface topography.

Under ideal circumstances, the individual atoms of a surface can be resolved and displayed. It should be noted, however, that STM images not only display the geometric structure of the surface, but also depend on the electronic density of states of the sample, as well as on special tip-sample interaction mechanisms which are not fully understood yet.

Although the STM itself does not need vacuum to operate (it works in air as well as under liquids), ultrahigh vacuum is required to avoid contamination of the samples from the surrounding medium.

1.5.2.2 Scanning Tunneling Spectroscopy (STS)

STS is an experimental technique which uses STM to probe (Fig. 7) the local density of electronic states (LDOS) and the band gap of surfaces and materials on surfaces at the atomic scale [49].

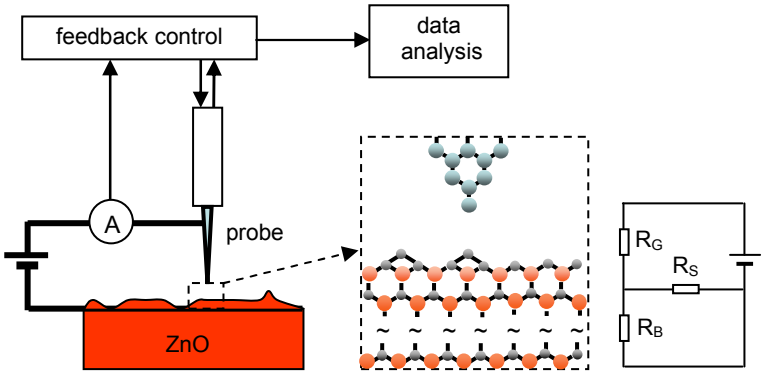

Fig. 7. *Scheme of STM and STS on a single crystal; the tip is probing the polar ZnO(0001)-Zn surface. Equivalent resistance of the tunnelling gap R_G, the partially metallised surface layer R_S, and the bulk material R_B.*

Generally, STS involves observation of changes in constant-current topographs with tip-sample bias, local measurement of the tunneling current versus tip-sample bias (I-V) curve, measurement of the tunneling conductance, dI/dV, or more than one of these. Since the tunneling current in a scanning tunneling microscope only flows in a region with diameter ~5 Å, STS is unusual in comparison with other surface spectroscopy techniques, which average over a larger surface region.

1.5.2.3 X-ray Photoelectron Spectroscopy (XPS)

XPS is a quantitative spectroscopic technique that measures the elemental composition, empirical formula, chemical state and electronic state of the elements that exist within a material. XPS spectra are obtained by irradiating a material with a beam of X-rays (Fig. 8) while simultaneously measuring the kinetic energy and number of electrons that escape from the top 1 to 10 nm of the

material being analyzed. XPS requires ultra-high vacuum (UHV) conditions.

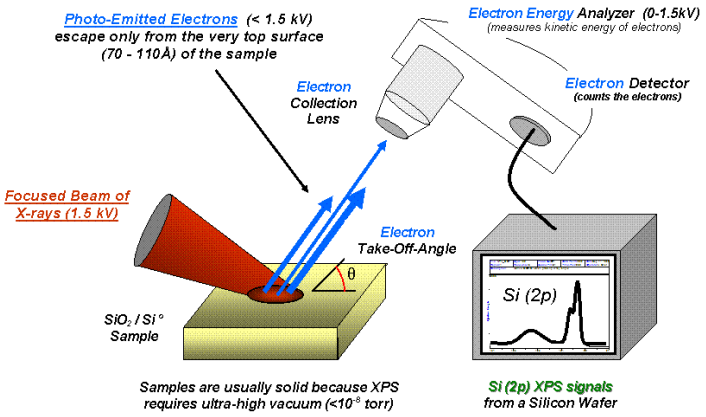

Fig. 8. *Basic components of a monochromatic XPS system (adapted from L. C. de Carvalho [50]).*

XPS is a surface chemical analysis technique that can be used to analyze the surface chemistry of a material in its "as received" state, or after some treatment, for example: fracturing, cutting or scraping in air or UHV to expose the bulk chemistry, ion beam etching to clean off some of the surface contamination, exposure to heat to study the changes due to heating, exposure to reactive gases or solutions, exposure to ion beam implant, exposure to ultraviolet light. XPS detection limits for most of the elements are in the parts per thousand range.

1.5.2.4 Temperature Programmed Desorption (TPD)

Thermal desorption spectroscopy (TDS), also known as temperature programmed desorption (TPD) is the method of observing desorbed molecules from a surface when the surface temperature is increased [51].

When molecules come in contact with a surface, they adsorb onto it, minimizing their energy by forming a chemical bond with the surface. The binding energy varies with the combination of the adsorbate and surface. If the surface is heated, at one point, the energy transferred to the adsorbed species will cause it to desorb. The temperature at which this happens is known as the desorption temperature. Thus TDS shows information on the binding energy.

Since TDS observes the mass of desorbed molecules, it shows what molecules are adsorbed on the surface. Moreover, TDS recognizes the different adsorption conditions of the same molecule from the differences between the desorption temperatures of molecules desorbing different sites at the surface, e.g. terraces vs. steps. TDS also obtains the amounts of adsorbed molecules on the surface from the intensity of the peaks of the TDS spectrum, and the total amount of adsorbed species is shown by the integral of the spectrum.

To measure TDS, one needs a mass spectrometer, such as a quadrupole mass spectrometer or a time-of-flight (TOF) mass spectrometer, under ultrahigh vacuum (UHV) conditions. The amount of adsorbed molecules is measured by increasing the temperature at a heating rate of typically 2 K/s to 10 K/s. Several masses may be simultaneously measured by the mass spectrometer, and the intensity of each mass as a function of temperature is obtained as a TDS spectrum.

The heating procedure is often controlled by the PID control algorithm, with the controller being either a computer or specialised equipment such as a Eurotherm.

A quantitative interpretation of the TDS results is usually done using the "Redhead" method [52], assuming the exponential prefactor and the desorption energy to be independent of the surface coverage.

1.6 Scope of the thesis

Considering the results over the last 15 years and the systematic work [53] done by my predecessor Dr. D. Brands, I specified the most valuable features of the Cu/ZnO catalyst in order to understand how these active sites are working. Then, based on these considerations, I formulated a concept and investigated it by surface science techniques.

In the last few decades, surface science techniques have drastically improved/developed in spatial/energetic resolution, spectral imaging/mapping, signal to noise ratio, and data processing. Modern surface science systems combine the reaction/catalysis chamber with a number of analysis techniques. This allows performing an *in-situ* or quasi *in-situ* analysis [42, 43] of the reacted surfaces. The technical progress makes it possible to investigate the “old” problem of Cu/ZnO active sites in details, and the amount of *in situ* studies of the problem increased substantially.

Chapter 2 describes the classical characterisation work on $Cu/ZnO/SiO_2$ silica supported catalyst [41]. The essence of this work is the effect of reduction temperature on Cu-Zn interaction. We found

that the increasing of reduction temperature up to 800 K leads to an increasing of metallic Cu-Zn interface area. This surface modification of activated catalyst is in a very good agreement with the LEIS study [22] performed on the highly surface sensitive ERISS machine at Technical University of Eindhoven.

The methanol synthesis activity and CO chemisorption measurements on our silica supported and unsupported systems were performed in the group of Prof. T. Yurieva (Boreskov Institute of Catalysis, Novosibirsk) at 20 bars and 493 K. The activation temperature was varied in the range 450 – 900 K. The performance of our catalyst is comparable with the industrial $Cu/ZnO/Al_2O_3$ catalyst and activity dependence on the reduction temperature correlates very well with the metal surface area.

The third chapter continues the characterisation of $Cu/ZnO/SiO_2$ catalyst in activation and reaction conditions by sophisticated in situ X-ray absorption techniques. This study was recently published and entitled as "Dynamic Cu/Zn interaction in SiO_2 supported methanol synthesis catalysts unravelled by in situ XAFS" [54]. It is important to note that the results of this study are complementary to the work described in second chapter. This structural EXAFS/XANES study was done in collaboration with groups of Prof. B. Weckhuysen (Utrecht University) and Prof. T. Yurieva (Boreskov Institute of Catalysis Novosibirsk) in the frame of the NWO Russian-Dutch collaboration project (# 047.015.004).

The fourth chapter deals with the small-angle neutron scattering (SANS) study [55] of isotopic enriched Cu/ZnO catalyst. The preliminary SANS measurements were done at St. Petersburg Nuclear Physics Institute within the above mentioned NWO project. The obtained results are very interesting and indicate that Cu clusters in the ZnO matrix contain a hydrogen core. We also found that these Cu clusters are surrounded by a hydrogen shell and its density is approximately 10 times smaller than in the core. Another surprising fact is that this reduced sample was exposed to air at room temperature for about one month before it was measured. Our results provide a new insight into the catalysis over Cu/ZnO surfaces. The refinement experiments of the preliminary SANS results confirmed that hydrogen is localized in Cu clusters. The hydrogen incorporation in the catalyst matrix could be a source of the atomic hydrogen for the catalyst re-activation.

The surface science study of ZnO and Cu/ZnO model catalyst, described in the fifth [42] and sixth [43] chapters, completes this PhD work. Fifth chapter describes the characterisation of the ZnO surfaces during exposure to reaction gases at elevated temperatures

[42]. It was found that the polar surface ZnO(0001)-Zn is rather active in methanol synthesis due to the highly defective surface. Since this surface is the lowest in view of surface free energy, its formation will be most favourable. Another interesting feature of this Zn-terminated surface is that it is depleted in Zn because of the dipole moment compensation. The interaction of ZnO surface with hydrogen leads to the formation of oxygen vacancies, so the surface gets more Zn-enriched. This could be related to the activity of the first industrial ZnO-based catalyst in methanol synthesis [56].

The sixth chapter deals with the model Cu/ZnO (0001)-Zn catalyst [43], and its behaviour during exposure to reactive gases. As in chapter 2, the main issue here is the Cu-Zn interaction in hydrogen at elevated temperatures of catalyst activation. Scanning Tunneling Microscopy and X-ray Photoelectron Spectroscopy results [43] clearly demonstrate a disappearance of Cu clusters from ZnO surface. Most plausible reason is the coverage of Cu clusters by ZnO_x species upon the increase of the reduction temperature. This behaviour is in accordance with thermodynamics due to the large difference in surface free energy between Cu (1825 mJ/m^2 [57]) and ZnO (90 mJ/m^2 [58]).

The Cu/ZnO-based catalyst structure was studied by the combination of structural [41, 54, 55] and surface sensitive techniques [42, 43]. Based on the results of this work, we conclude the surface of activated Cu/ZnO catalyst consists of alloyed Zn-Cu sites and that structure is stabilised by the hydrogen incorporated in the catalyst matrix. The modification behaviour of catalyst structure upon the reduction temperature determines the highest Zn-Cu interface area formed at about 750-800 K of reduction temperature. It is suggested that the activated structure will remain active at about 500 K of methanol synthesis temperature mainly because of the available atomic hydrogen trapped in the matrix.

References

1. Methanol Institute Homepage. http://www.methanol.org (accessed 2012).
2. G.A. Olah, A. Goeppert, G.K.S. Prakash, *Beyond Oil and Gas: The Methanol Economy. Wiley-VCH Verlag GmbH*, 2006.
3. *BP statistical review of world energy*, 2004.
4. World Nuclear Association Homepage. http://www.world-nuclear.org (accessed 2012).
5. G.C. Chinchen, K. Mansfield and M.S. Spencer, *CHEMTECH*, 1990, 692.
6. Johnson Matthey Homepage. http://www.jmcatalysts.com (accessed 2012).
7. Haldor Topsøe Homepage. http://www.haldortopsoe.com (accessed 2012).
8. Y.B. Kagan, L.G. Liberov, E.V. Slivinskii, S.M. Loktev, G.I. Lin, A.Y. Rozovskii and A.N. Bashkirov, *Dokl. Akad. Nauk SSSR,* 1975, 221, 1093.
9. A.Y. Rozovskii and G.I. Lin, *Top. Catal.*, 2003, 22, 137.
10. G.C. Chinchen, P.J. Denny, D.G. Parker and M.S. Spencer, *Appl. Catal.*, 1987, 30, 333.
11. G.C. Chinchen, K.C. Waugh and D.A. Whan, *Appl. Catal.*, 1986, 25, 101.
12. P.B. Rasmussen, P.M. Holmblad, T. Askgaard, C.V. Ovesen, P. Stoltze, J.K. Norskov and I. Chorkendorff, *Catal. Lett.*, 1994, 26, 373.
13. J. Yoshihara and C.T. Campbell, *J. Catal.*, 1996, 161, 776.
14. M.S. Spencer, *Catal. Lett.*, 1998, 50, 37.
15. S. Mehta, G.W. Simmons, K. Klier and R.G. Herman, *J. Catal.*, 1979, 57, 339.
16. K. Klier, *Adv. Catal.*, 1982, 31, 243.
17. Y. Okamoto, K. Fukino, T. Imanaka and S. Teranishi, *J. Phys. Chem.*, 1983, 87, 3747.
18. N.Y. Topsøe and H. Topsøe, *J. Mol. Catal. A-Chem.*, 1999, 141, 95.
19. T. Fujitani and J. Nakamura, *Appl. Catal. A*, 2000, 191, 111.
20. Y. Choi, K. Futagami, T. Fujitani and J. Nakamura, *Catal. Lett.*, 2001, 73, 27.
21. J. Nakamura, Y. Choi and T. Fujitani, *Top. Catal.*, 2003, 22, 277.
22. W.P.A. Jansen, J. Beckers, J.C. v.d. Heuvel, A.W. Denier v.d. Gon, A. Bliek and H.H. Brongersma, *J. Catal.*, 2002, 210, 229.
23. S.A. French, A.A. Sokol, S.T. Bromley, C.R.A. Catlow, S.C. Rogers, F. King and P. Sherwood, *Angew. Chem., Int. Ed.*, 2001, 40, 4437.
24. R. Burch, S. Golunski and M.S. Spencer, *Catal. Lett.*, 1990, 5, 55.

25. M.M. Günter, T. Ressler, B. Bems, C. Buscher, T. Genger, O. Hinrichsen, M. Muhler and R. Schlogl, *Catal. Lett.*, 2001, 71, 37.
26. J.B. Wagner, P.L. Hansen, A.M. Molenbroek, H. Topsøe, B.S. Clausen and S. Helveg, *J. Phys. Chem. B*, 2003, 107, 7753.
27. J.D. Grunwaldt, A.M. Molenbroek, N.Y. Topsøe, H. Topsøe and B.S. Clausen, *J. Catal.*, 2000, 194, 452.
28. P.L. Hansen, J.B. Wagner, S. Helveg, J.R. Rostrup-Nielsen, B.S. Clausen and H. Topsøe, *Science*, 2002, 295, 2053.
29. S.V. Ketchik, T.P. Minyukova, L.I. Kuznetsova, L.M. Plyasova, T.M. Yurieva and G.K. Boreskov, *React. Kin. Catal. Lett.*, 1982, 19, 345.
30. T.M. Yurieva, L.M. Plyasova, T.A. Kriger, V.I. Zaikovskii, O.V. Makarova and T.P. Minyukova, *React. Kin. Catal. Lett.*, 1993, 51, 495.
31. D. Stirling, F.S. Stone and M.S. Spencer, *Stud. Surf. Sci. Catal.*, 1993, 75, 1507.
32. T.M. Yurieva, L.M. Plyasova, T.A. Kriger and O.V. Makarova, *Kinet. Catal.*, 1995, 36, 707.
33. L.M. Plyasova, L.P. Solovyeva, T.A. Krieger, O.V. Makarova and T.M. Yurieva, *J. Mol. Catal. A-Chem.*, 1996, 105, 61.
34. E.K. Poels and D.S. Brands, *Appl. Catal. A*, 2000, 191, 83.
35. D.O. Klenov, G.N. Kryukova and L.M. Plyasova, *J. Mater. Chem.*, 1998, 8, 1665.
36. T.M. Yurieva, L.M. Plyasova, V.I. Zaikovskii, T.P. Minyukova, A. Bliek, J.C. v.d. Heuvel, L.P. Davydova, I.Y. Molina, M.P. Demeshkina, A.A. Khassin and E.D. Batyrev, *Phys. Chem. Chem. Phys.*, 2004, 6, 4522.
37. D.S. Brands, E.K. Poels, T.A. Krieger, O.V. Makarova, C. Weber, S. Veer and A. Bliek, *Catal. Lett.*, 1995, 36, 175.
38. J. Nakamura, I. Nakamura, T. Uchijima, Y. Kanai, T. Watanabe, M. Saito and T. Fujitani, *Catal. Lett.*, 1995, 31, 325.
39. J.E. Bailie, C.H. Rochester and G.J. Millar, *Catal. Lett.*, 1995, 31, 333.
40. F.T. v.d. Scheur and L.H. Staal, *Appl. Catal. A*, 1994, 108, 63.
41. E.D. Batyrev, J.C. v.d. Heuvel, J. Beckers, W.P.A. Jansen and H.L. Castricum, *J. Catal.*, 2005, 229, 136.
42. E.D. Batyrev and J.C. v.d. Heuvel, *Phys. Chem. Chem. Phys.*, 2011, 13, 13127.
43. E.D. Batyrev, N. Raveendran Shiju and G. Rothenberg, *J. Phys. Chem. C*, 2012, 116, 19335.
44 B. Jacrot, *Reports on Progress in Physics* 1976, 39, 911.
45. K. Siegbahn and K.I. Edvarson, *Nuclear Physics,* 1956, 1, 137.
46. R. Young, J. Ward, R. Your, *Phys. Rev. Lett.*, 1971, 27, 922.

47. G. Binnig and H. Rohrer, *US Patent* 4343993, 1982; *IBM J. Res. Dev.* 1986, 30, 4, 355.
48. http://en.wikipedia.org/wiki/Scanning_tunneling_microscope (accessed 2012).
49. K. Oura, V. G. Lifshits, A. A. Saranin, A. V. Zotov, and M. Katayama, *Surface Science: An Introduction, Berlin: Springer-Verlag*, 2003.
50. http://en.wikipedia.org/wiki/X-ray_photoelectron_spectroscopy (accessed 2012).
51. J. W. Niemantsverdriet, *Spectroscopy in Catalysis*, VCH Weinheim, 1993.
52. P.A. Redhead, *Vacuum*, 1962, 12, 203.
53. D. Brands, *Ph.D. thesis*, University of Amsterdam, 2001, ISBN 90-9011520-X.
54. D. Grandjean, V. Pelipenko, E.D. Batyrev, J.C. v.d. Heuvel, A.A. Khassin, T.M. Yurieva and B.M. Weckhuysen, *J. Phys. Chem. C*, 2011, 115, 20175.
55. V.A. Trounov, A.E. Sokolov, V.T. Lebedev, O.P. Smirnov, A.I. Kurbakov, J.C. v.d. Heuvel, E.D. Batyrev, T.M. Yurieva, L.M. Plyasova and Gy. Török, *Sol. State Phys.*, 2006, 48, 1291.
56. A. Mittasch and M. Pier, *US patent* ref. no. 1.569.775. filed Jan. 12, 1926.
57. F.R. de Boer, R. Boom, W.C.M. Mattens, A.R. Miedema, and A.K. Niessen, *Cohesion in Metals, North-Holland, Amsterdam*, 1988.
58. S.H. Overbury, P.A. Bertrand, and G.A. Somorjai, *Chem. Rev.,* 1975, 75, 547.